The interplay between slippage and apparent viscosity at nanoscale solid-liquid interfaces with different wettability

Deborah Ortiz-Young[1, 2 +], Hsiang-Chih Chiu[1 +], Suenne Kim[1], Kislon Voïtchovsky[3], and Elisa Riedo[1]*

+ Contributed Equally

[1] School of Physics, Georgia Institute of Technology, 837 State Street, Atlanta, GA 30332-0430, USA

[2] School of Chemistry, Georgia Institute of Technology, 901 Atlantic Avenue, Atlanta, GA 30332-0430, USA

[3] Institute of Materials, Ecole Polytechnique Fédérale de Lausanne, 1015 Lausanne, Switzerland

*email: elisa.riedo@physics.gatech.edu

Understanding and manipulating fluids at the nanoscale is a matter of growing scientific and technological interest. Interfacial and nano-confined liquid flow is relevant for biology[1,2], tribology[3], nanofluidics, and high-resolution 3D, 2D-printing[4]. Here, experiments show that the viscous shear forces in nano-confined water can be orders of magnitudes larger than in bulk water if the confining surfaces are hydrophilic, whereas they greatly decrease when the surfaces are increasingly hydrophobic. This decrease of viscous forces is quantitatively explained with a simple model that includes the slip velocity at the water-surface interface. The same effect is observed in the energy dissipated by a tip vibrating in water, perpendicularly to a surface. Comparison of the experimental data with the model shows that interfacial viscous forces and compressive dissipation in nano-confined water can decrease up to two orders of magnitude due to slippage. These results offer a new understanding of interfacial fluids, which can be used to control flow at the nanoscale.

Crucial for the understanding of fluid flow in nano-size spaces is the liquid-solid interface[5]. Confined fluids exhibit unique structural, dynamical, electrokinetic, and mechanical properties that are different from those of the bulk[6-10]. It is now well-known that liquids confined between surfaces, especially at gaps below a few nanometers, can present a dramatic increase in their viscosity[6,7,11,12]. Experiments and theory have shown that the viscosity of water confined between hydrophilic surfaces increases with confinement, reaching values orders of magnitude higher than bulk water for sub-nanometer confinement[6,7,11,12]. It is also clear that the usual no-slip boundary condition, i.e. zero fluid velocity at the motionless surface, is not universal and experiments and computer simulations have proved that liquid molecules can slip and have a non-zero velocity at a still solid surface [13,14,15]. Furthermore, several studies have indicated that the amount of liquid slip strongly depends on the morphology and chemistry of the stationary solid surface[16,17]. However, no experiments have so far investigated the interrelationship between the viscosity of nanoconfined water, the wettability of the confining surfaces, and the interface slippage.

Here, we present experiments using an atomic force microscope (AFM) showing that the interfacial viscous forces in nanoconfined water increase substantially for more hydrophilic confining surfaces, and for increasing confinement. We use a selection of atomically flat surfaces exhibiting different wetting properties and compare, as a function of confinement, viscous forces, energy dissipation and water slippage. This approach enables use to unambiguously single out the influence of surface properties (wetting) on the measured viscosity/dissipation. A comparison of the experimental data with a modified form of the Newtonian definition of viscosity that includes slippage demonstrates that the origin of this increase in viscous force (and apparent viscosity) is a reduced slippage at the surface. On the other hand, the intrinsic viscosity

of nanoconfined water is not affected by surface hydrophilicity at any confinement size, until the last water layer close to the surface, and remains extremely high compared to that of bulk water. The same modified Newtonian model is then used to explain the dependence of energy dissipation on surface wettability in dynamic AFM experiments in water. For a given confinement size *d,* both the ratios of the viscous forces and energy dissipation measured on a variety of surfaces and on a surface with zero slip length *b*, are equal to $d/(b+d)$, as predicted by the definition of viscosity for a shear velocity gradient of $v_{shear}/(d+b)$. These measurements reveal the relationship between water viscous interfacial forces and slippage, as well as the link between the nano-confined water apparent viscosity and wettability. These results have important implications in nanotechnology and bio-nanoscience where the interaction in water between surfaces and objects at the nanoscale is mediated by the properties and the dynamic behavior of water.

By using an AFM, we have measured the shear viscous force, F_{shear}, experienced in water by a nano-size AFM tip while it is sheared parallel to a atomically smooth solid surface, as a function of the tip-surface distance, *d* (see Fig. 1a). These viscous force curves, $F_{\text{shear}}(d)$, have been measured for five surfaces with different wettabilities, characterized by the static contact angle of water, θ (see Supplementary Information). We find a strong dependence of the viscous force on wettability, with force values varying from one surface to another one up to an order of magnitude at $d \approx 0.3$ nm, corresponding approximately to one layer of water molecules on the solid surface. Viscous (shear) and solvation (normal) forces at the tip are measured simultaneously as a function of the tip-surface distance by detecting, respectively, the torsion and bending of a rectangular cantilever rigidly attached to the silicon tip, while it approaches a smooth solid surface in deionized ultra-filtered (DIUF) water (see Fig. 1 and Methods part).

During the approach, the cantilever is laterally sheared by means of a lock-in amplifier with a shearing amplitude and frequency of 0.9 nm and 1 kHz, respectively. We remark that for this shearing speed, v_{shear} = 900 nm/s, the lateral force is mainly viscous, as measured from the 90^{o} phase shift with the displacement[7]. The atomically smooth solid surfaces used in the viscosity measurements are, from the most to the least hydrophilic, on Mica, Graphene Oxide (GO), Silicon, diamond like carbon (DLC), and Highly Oriented Pyrolytic Graphite (HOPG) (see Methods part and Supplementary Information for more details). The static contact angles have been characterized by imaging a small water droplet on the different surfaces (See Supplementary Information). A large contact angle indicates a poorly wetting surface, also referred as hydrophobic surface for the case of water, whereas vanishing contact angles indicate wetting surfaces, also called hydrophilic surfaces for water.

Figure 2 shows the shear viscous forces acting on an AFM tip when it approaches surfaces with different wettability in water as a function of the tip-surface separation. For each surface, the curves are averaged over multiple force curves as described in the Supplementary Information. For all the investigated surfaces, the viscous force F_{shear} approaches a value close to zero within the experimental error at $d > 3$ nm, and increases dramatically for d approaching zero. We remark that for larger distances the measured F_{shear} is almost zero because the viscosity of bulk water is too small to be measured with our instrument. On the other hand, when the tip is very close to the surface, $d < 2$ nm, the increased F_{shear} experienced by the tip at its apex is large enough to be detected as the torsion of the cantilever, as already reported in previous studies performed on Mica[6,7,11,12]. Finally, much higher shear forces can be observed when the tip indents the solid's surface. Nevertheless, although all the investigated solid surfaces give rise to a qualitatively similar trend in viscous forces, for fixed tip-surface distances, the viscous force

clearly decreases going from Mica, to GO, DLC, Si, and HOPG, respectively. To understand the origin of this decrease in the observed viscous force as a function of the interface material, we have characterized the wettability of the surfaces with static contact angle measurements. The static contact angles of water for the investigated surfaces are the following: $\theta_{Mica} = 4 \pm 3°$, $\theta_{GO} = 48 \pm 3°$, $\theta_{DLC} = 66 \pm 6°$, $\theta_{Si} = 76 \pm 4°$, and $\theta_{HOPG} = 85 \pm 4°$. As shown in Fig. 2, larger viscous forces correlate with smaller contact angles (more hydrophilic/wetting surfaces). The observed relationship between contact angle and interfacial viscous force suggests that the interfacial slippage, which is known to often increase with the static contact angle of the surface[18], may play a crucial role in the interfacial viscous forces. In order to demonstrate this hypothesis and to extract more quantitative information from these results, a modified Newtonian definition of viscosity is used for further analysis.

For a Newtonian fluid confined between two flat plates separated by a distance d, the shear force required to slide one plate parallel to a stationary one is proportional to the gradient of the fluid velocity in the direction perpendicular to the plates, $\partial v_x/\partial z$ (see Fig. 1b):

$$F_{shear}/A = \eta \cdot (\partial v_x/\partial z) \quad (1)$$

The proportionality factor, η, is defined as the viscosity of the liquid, while A is the area of the shearing plate. If the velocity profile is simply linear with no slippage, as shown in Fig. 1b, we have $\partial v_x/\partial z = v_{shear}/d$, where v_{shear} is the shear velocity of the top plate. On the other hand, for a linear velocity profile with a finite slip length b as illustrated in Fig. 1c, we will have:

$$\partial v_x/\partial z = v_{shear}/(d + b) \quad (2).$$

As a first approximation, we can consider that the velocity profile of water between the AFM tip and the solid surface to be linear. Furthermore, for $d < 2$ nm and water the tip apex can be approximated to be a planar surface, as described in previous work[6]. Then we can combine

equations (2) and (1) to obtain the ratio between the shear force in water close to surface B with $b \neq 0$ and surface A with $b=0$ (see Fig. 1):

$$\frac{F_{\text{shear}}^{b}(d)}{F_{\text{shear}}^{b=0}(d)} = \frac{\eta^{B}(d)}{\eta^{A}(d)} \frac{d}{d+b} \qquad (3),$$

where $F_{\text{shear}}^{b}(d)$ and $\eta^{B}(d)$ are respectively the shear viscous force and the viscosity as a function of the tip-surface distance measured in water close to a surface with slip length equal to b. We note that in equation (3) the viscosity is a function of d, since it is known that for nano-confined water the viscosity can be confinement dependent[6,7,11,12]. At present, it is unknown the behavior of interfacial water viscosity for confining surfaces with different degree of wettabilities (and different slip lengths), thus *a priori* we don't know $\eta^{B}(d)$. Equation (3) indicates that the measured viscous forces on different surfaces depend on two related but distinguished phenomena: the intrinsic viscosity of nano-confined water, which may change depending on the confining surfaces, and the slippage of water at the solid surface interface, which is already known to depend on properties such as the contact angle[18]. Since the slip length of hydrophilic Mica is almost zero accordingly to a previous study[19], we can assume that the viscous force measured on Mica is indeed $F_{\text{shear}}{}^{b=0}(d)$ and the viscosity is: $\eta^{Mica}(d) = \frac{F_{shear}^{b=0}}{A} \cdot \frac{d}{v_{shear}}$. Equation (3) together with the viscous shear forces measured on Mica is then used to fit the viscous forces measured on all the other surfaces with unknown $\eta^{B}(d)$. As initial working hypothesis we have assumed that for every surface and d the viscosity remains the same as for Mica, $\eta^{any-surface}(d) = \eta^{Mica}(d)$, and we have then fit all the shear viscous forces for the different surfaces with the Equation:

$$\frac{F_{\text{shear}}(d)}{F_{\text{shear}}^{Mica}(d)} = \frac{d}{d+b} \quad (4),$$

leaving b as a free fitting parameter, to be compared with data measured or calculated in literature with different methods[18, 19, 20, 21]. The fitting process is illustrated in Fig. 3, where the experimental $F_{\text{shear}}(d)$ curves measured on partially hydrophobic HOPG, DLC, GO (Fig. 3b-3d)), and Si (shown in Fig. S5b of Supplementary Information), are fitted using the viscous force curve acquired on hydrophilic Mica (Fig. 3a) between $d \approx 0.3$ - 3 nm as the zero slippage viscous curve. The values of slip length obtained from this fitting procedure are the following: b = 0.24±0.38 nm, 0.55±1.37 nm, 1.0±1.7 nm, and 12.0±3.3 nm, for GO, DLC, Si and HOPG, respectively (See Supplementary Information for the fitting details). These slip lengths values are then plotted as a function of the static contact angle of the corresponding surface in Supplementary Fig. S5. First, these values are in good agreement with existing experimental or theoretical values found in literature[18,20,21,22,23] (see Table S3). Second, the good superposition of the fitting curves with the experimental data points confirms that equation (4) is able to capture the physics behind the different observed viscous behaviors, demonstrating that the striking variations in the viscous forces at the interface are indeed related to different water slippages at the interface, while the intrinsic viscosity of nano-confined water remains the same independently of surface hydrophilicity at any confinement d.

Figure 4a shows for $d \approx 0.3$ and 0.7 nm the measured $\frac{F_{\text{shear}}(d)}{F_{\text{shear}}^{Mica}(d)}$ and $\frac{\eta(d)}{\eta_{bulk}}$ as a function of the static contact angle of the corresponding surface, where η_{bulk} is the viscosity of bulk water at room temperature, and $\eta\ (d) = \frac{F_{\text{shear}}}{A}\frac{d+b}{v_{shear}}$ being b the slip length of the investigated surface. In order to prove the generality of our conclusions, we performed AFM experiments with a tip oscillating

perpendicularly to a surface, in the standard configuration used in non-contact, dynamic mode AFM. We then recorded the energy dissipation, E_T, due to viscous losses as the tip oscillates in water close to a variety of solid surfaces (see Methods and Supplementary Information for more details). Previous work has shown that such losses are correlated with the static contact angle of the surfaces[24,25], but the physical origin of this link has to date not been explained. Motivated by our new understanding, we argue that the average energy costs associated with the subsequent approach and retraction of a tip vertically oscillating within ~1 nm from a surface (interface) can be explained water slippage and is hence proportional to the viscous forces at that interface, as modeled in equation (4):

$$\frac{E_{\mathrm{T}}^{b}(d)}{E_{\mathrm{T}}^{b=0}(d)} = \frac{d}{d+b(\theta)} = \frac{F_{\mathrm{shear}}^{b}(d)}{F_{\mathrm{shear}}^{b=0}(d)} \qquad (5),$$

where $E_T^{b=0}$ is the energy dissipation measured on Mica, and E_T^{b} is the energy dissipation measured on a surface with a given slip length and contact angle. We then obtain the slip length as a function of the contact angle of the surface over which the energy dissipation is measured by using equation (5) in the form $b(\theta) = \frac{E_T^{\mathrm{Mica}}}{E_T(\theta)} - 1$, for d = 1 nm. The results, presented as open squares in the Supplementary Figure S5 along with the values of b vs. contact angle as found from the fitting of the shear viscous forces shown in Fig 3, display a clear agreement between the viscous force shearing experiments and the compressive dissipation experiments, demonstrating that in both cases the water slip length is at the origin of the wettability dependent viscous dissipation. Significantly, these results also provide a new framework for interpreting AFM experiments in water. Furthermore, in Fig. 4b we plotted for d = 1 nm the ratio between the viscous force on an arbitrary surface and on Mica, as well as the ratio of the compressive energy dissipation on an arbitrary surface and on Mica, as a function of the slip length of the

corresponding surface. These ratios fall on a single master curve equal to $d/(b + d)$. Figure 4a and 4b show the main conclusive results of this study, namely the relationship between water interfacial viscous forces (and energy dissipation) and slippage at that interface. In particular our results demonstrate that interfacial viscous forces and the dissipated energy during compression in nano-confined water can decrease of up to two orders of magnitude due to water slippage, whereas the intrinsic viscosity (Fig. 4a top panel) remains extremely high compared to bulk water and independent of surface hydrophilicity for every confinement size. The origin of such a large viscosity of nanoconfined water is not completely understood. Certainly it is important to remark that we are dealing with only 3-4 water atomic layers where water may undergo structural changes such as layering effects, a slow-down of water dynamics due to confinement, or nano-jamming effects.

We remark that although these results are possibly limited to surfaces that are ultra-smooth and with hydrophobicity below 90^{o}, the conclusions provide a new general understanding of interfacial phenomena, which may have an impact in a wide range of studies and applications.

In summary, we have studied water interfacial viscosity on substrates with different wettability. Our results demonstrate that boundary viscous forces are related to slippage processes, which in turn can depend on the wettability of the interfacial surface. A modified form of the Newtonian definition of viscosity, which takes the fluid slip into account, is successfully used to explain that the decrease of the interfacial viscous forces with increasing hydrophobicity is due to a respective increase in slip length, whereas the intrinsic viscosity of nano-confined water remains the same for all the surfaces investigated here, at any confinement size. The same model is also used to quantitatively explain the so far unclear relationship between surface wettability and energy dissipation in dynamic AFM experiments. Beyond the reign of water, this new

understanding of the interplay between interfacial viscosity, wettability and boundary slip might explain the change in glass transition temperature of very thin polymer films as a function of the polymer wettability of the substrate[26]. Finally, this work opens up new strategies to investigate the hydration layers in complex systems such as proteins[1] and cytoskeletal filaments[27].

METHODS

Water Purity

Deionized ultra-filtered (DIUF) water was purchased from Fischer Scientific, and the purity was confirmed with an AB30 Conductivity Meter (Fischer Scientific). The measurement indicated a resistance of 18 MΩ, corresponding to an ion concentration of less than 0.04 parts per million.

Viscous Force Measurements

The lateral viscous force experiments were performed in DIUF water with an AFM (Picoplus 5500, Agilent) at room temperature. A silicon AFM cantilever with typical normal and lateral spring constants equal to $k_N \approx 3$ to 5 N/m and $k_T \approx 50$ to 120 N/m, respectively, are used. The tip radius is approximately 40 nm, as measured by Scanning Electron Microscope (JOEL JSM-5910) imaging after each experiment. The AFM tip approaches the hard solid surface at a vertical speed of 0.2 nm/s. The shearing frequency, 1 kHz, and amplitude, 0.9 nm, are controlled by a lock-in amplifier. See also Ref. [6, 7]. For each surface, several lateral and normal force vs. separation d curves were obtained. These force curves are averaged as shown in Fig. 2. See Supplementary Information for more details.

Muscovite Mica and Highly Oriented Pyrolytic Graphite were prepared for experiments via the tape-refresh method. GO was synthesized by oxidation of epitaxial graphene using the Hummers method[28]. Si and DLC surfaces were cleaned by sonication with various organic solvents and dried with compressed nitrogen gas, as reported in Supplementary Information. The contact angle was measured with a Contact Angle Meter (Phoenix 150, SEO).

In the literature, the slip length of water on HOPG is reported to be 8±2 nm[20], which is in good agreement with the value of 12±4 nm found here.

Energy Dissipation Measurements

Measurements of the local energy dissipation were performed with a Multimode Nanoscope IIIa AFM (Digital Instruments) equipped with an external lock-in amplifier. The AFM was operated in amplitude-modulation mode with the cantilever driven close to its resonance in water. The tip and sample were fully immersed in ultrapure water. While imaging, the system was adjusted so as to ensure that most of the tip oscillation (and damping) occurs within the interfacial water at the surface of the solid. This is typically achieved using vibration amplitudes of ~1nm and 'soft' scanning setpoints[24]. The tip vibration amplitude and phase (phase lag with the driving vibration) were acquired for each point (pixel) of the imaged sample. Knowing the cantilever stiffness and Q-factor (calculated from the cantilever thermal spectrum[29]), the tip local energy dissipation is calculated using the simple harmonic oscillator formalism[30]. The energy dissipation values presented in Fig. 4 represent averages of the calculated local energy dissipation over areas covering several tens of nanometers squares. We investigated energy dissipation on Mica, silicon oxide, aluminum oxide, strontium titanate, optical grad calcite, silicon carbide, titanium dioxide, fluorite, and HOPG, with contact angles of < 20°, 24°, 58.3°, 71°, 74°, 80.1°, 80.5°, 86°, and

90.9°, respectively. Details of the AFM measurements and the preparation of the different samples used here are presented in the Supplementary Information.

Mitigation of errors

Nanoscale measurements are inherently sensitive to surface imperfection such as nanoscale singularities and contamination. Here we take several steps to mitigate these problems. First, we used atomically smooth surfaces, such as single crystals, with consistent surface cleaning procedures, and conducted the AFM measurements in clean and controlled environment. Possible contaminations (e.g. due to hydrocarbon molecules) tend to induce dramatic effects on the measurements, which can be unambiguously discarded. Furthermore, all the measurements were repeated several times on different locations of each sample (See SI).

Finally complementary nanoscale approaches were conducted independently in two different laboratories, always yielding the same general trend, which can be explained by our simple model.

Acknowledgements

D. Ortiz, H.-C.C. E.R. acknowledge the financial support of the Office of Basic Energy Sciences DOE (DE-FG02-06ER46293). E.R. acknowledges the National Science Foundation NSF (DMR-0120967 and DMR-0706031) for partial support. KV acknowledges funding from the Swiss National Science Foundation (Ambizione Award). All the authors would like to thank Lyderic Bocquet and Francesco Stellacci for stimulating discussions.

Reference

1 Craighead, H. G. Nanoelectromechanical systems. *Science* **290**, 1532-1535 (2000).

2 Han, J. & Craighead, H. G. Separation of long DNA molecules in a microfabricated entropic trap array. *Science* **288**, 1026-1029 (2000).

3 Socoliuc, A. *et al.* Atomic-Scale Control of Friction by Actuation of Nanometer-Sized Contacts. *Science* **313**, 207-210 (2006).

4 Sinha, P. K. & Wang, C. Y. Pore-network modeling of liquid water transport in gas diffusion layer of a polymer electrolyte fuel cell. *Electrochim. Acta* **52**, 7936-7945, (2007).

5 Carrasco, J., Hodgson, A. & Michaelides, A. A molecular perspective of water at metal interfaces. *Nature Mater.* **11**, 667-674 (2012).

6 Li, T. D., Gao, J. P., Szoszkiewicz, R., Landman, U. & Riedo, E. Structured and viscous water in subnanometer gaps. *Phys. Rev. B* **75**, 115415 (2007).

7 Li, T. D. & Riedo, E. Nonlinear viscoelastic dynamics of nanoconfined wetting liquids. *Phys. Rev. Lett.* **100**, 106102 (2008).

8 Mitsui, T., Rose, M. K., Fomin, E., Ogletree, D. F. & Salmeron, M. Water Diffusion and Clustering on Pd(111). *Science* **297**, 1850-1852 (2002).

9 N. Giovambattista, P.J. Rossky and P.G. Debenedetti, Computational Studies of Pressure, Temperature and Surface Effects on the Structure and Thermodynamics of Confined Water. *Annu. Rev. Phys. Chem*., **63,** 179, 2012**.**

10 Wang, H.-J., Xi, X.-K., Kleinhammes, A. & Wu, Y. Temperature-Induced Hydrophobic-Hydrophilic Transition Observed by Water Adsorption. *Science* **322**, 80-83 (2008).

11 Khan, S. H., Matei, G., Patil, S. & Hoffmann, P. M. Dynamic Solidification in Nanoconfined Water Films. *Phys. Rev. Lett.* **105**, 106101 (2010).

12 Goertz, M. P., Houston, J. E. & Zhu, X. Y. Hydrophilicity and the viscosity of interfacial water. *Langmuir* **23**, 5491-5497 (2007).

13 Barrat, J. L. & Bocquet, L. Large slip effect at a nonwetting fluid-solid interface. *Phys. Rev. Lett.* **82**, 4671-4674 (1999).

14 van der Heyden, F. H. J., Bonthuis, D. J., Stein, D., Meyer, C. & Dekker, C. Power generation by pressure-driven transport of ions in nanofluidic channels. *Nano Lett.* **7,** 1022-1025 (2007).

15 Schoch, R. B., Han, J. Y. & Renaud, P. Transport phenomena in nanofluidics. *Rev. Mod. Phys.* **80**, 839-883 (2008).

16 Cottin-Bizonne, C., Barrat, J. L., Bocquet, L. & Charlaix, E. Low-friction flows of liquid at nanopatterned interfaces. *Nature Mater.* **2**, 237-240 (2003).

17 Neto, C., Evans, D. R., Bonaccurso, E., Butt, H. J. & Craig, V. S. J. Boundary slip in Newtonian liquids: a review of experimental studies. *Rep. Prog. Phys.* **68**, 2859-2897 (2005).

18 Huang, D. M., Sendner, C., Horinek, D., Netz, R. R. & Bocquet, L. Water Slippage versus Contact Angle: A Quasiuniversal Relationship. *Phys. Rev. Lett.* **101**, 226101 (2008).

19 Israelachvili, J. N. Measurement of the viscosity of liquids in very thin films. *J. Colloid Interface Sci.* **110**, 263-271 (1986).

20 Maali, A., Cohen-Bouhacina, T. & Kellay, H. Measurement of the slip length of water flow on graphite surface. *Appl. Phys. Lett.* **92**, 053101-053102 (2008).

21 Sendner, C., Horinek, D., Bocquet, L. & Netz, R. R. Interfacial Water at Hydrophobic and Hydrophilic Surfaces: Slip, Viscosity, and Diffusion. *Langmuir* **25**, 10768–10781 (2009).
22 Lichter, S., Martini, A., Snurr, R. Q. & Wang, Q. Liquid Slip in Nanoscale Channels as a Rate Process. *Phys. Rev. Lett.* **98**, 226001 (2007).
23 Thompson, P. A. & Troian, S. M. A general boundary condition for liquid flow at solid surfaces. *Nature* **389**, 360-362 (1997).
24 Voitchovsky, K., Kuna, J. J., Contera, S. A., Tosatti, E. & Stellacci, F. Direct mapping of the solid-liquid adhesion energy with subnanometre resolution. *Nature Nanotech.* **5**, 401-405, (2010).
25 Kuna, J. J. *et al.* The effect of nanometre-scale structure on interfacial energy. *Nature Mater.* **8**, 837-842, (2009).
26 Yang, Z., Fujii, Y., Lee, F. K., Lam, C.-H. & Tsui, O. K. C. Glass Transition Dynamics and Surface Layer Mobility in Unentangled Polystyrene Films. *Science* **328**, 1676-1679 (2010).
27 Reátegui, E. & Aksan, A. Effects of the Low-Temperature Transitions of Confined Water on the Structures of Isolated and Cytoplasmic Proteins. *J. Phys. Chem. B* **113**, 13048-13060 (2009).
28 Kim, S. *et al.* Room-temperature metastability of multilayer graphene oxide films. *Nature Mater.* **11**, 544-549 (2012).
29 Hutter, J. L. & Bechhoefer, J. Calibration of atomic-force microscope tips. *Rev. Sci. Instrum.* **64**, 1868-1873 (1993).
30 Cleveland, J. P., Anczykowski, B., Schmid, A. E. & Elings, V. B. Energy dissipation in tapping-mode atomic force microscopy. *Appl. Phys. Lett.* **72**, 2613-2615 (1998).

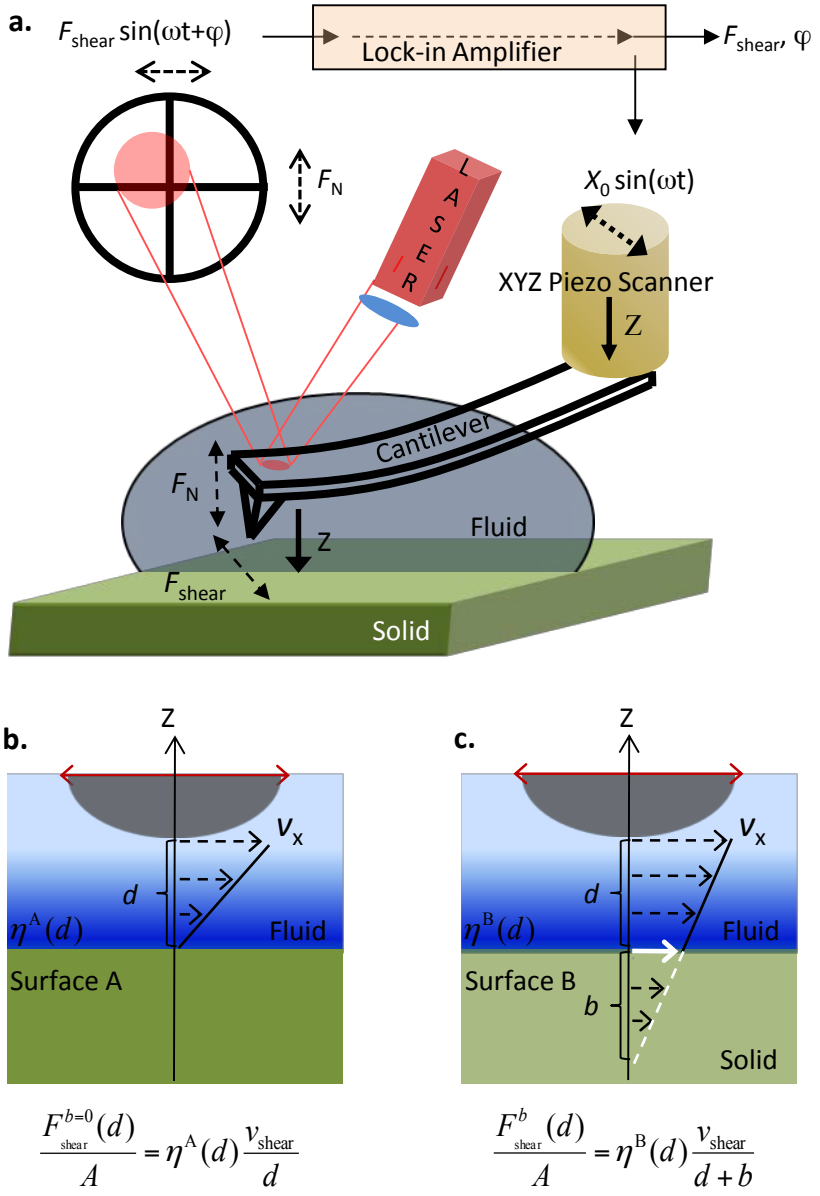

Figure 1. The experimental setup and schematics of the boundary conditions. a, Overview of the experimental setup. **b,** Fluid velocity profile for a no-slip boundary condition (b=0) and for **c,** a finite slip boundary condition ($b\neq0$). The slip length is defined as the distance between the solid-fluid interface and the point where the velocity profile extrapolates to zero.

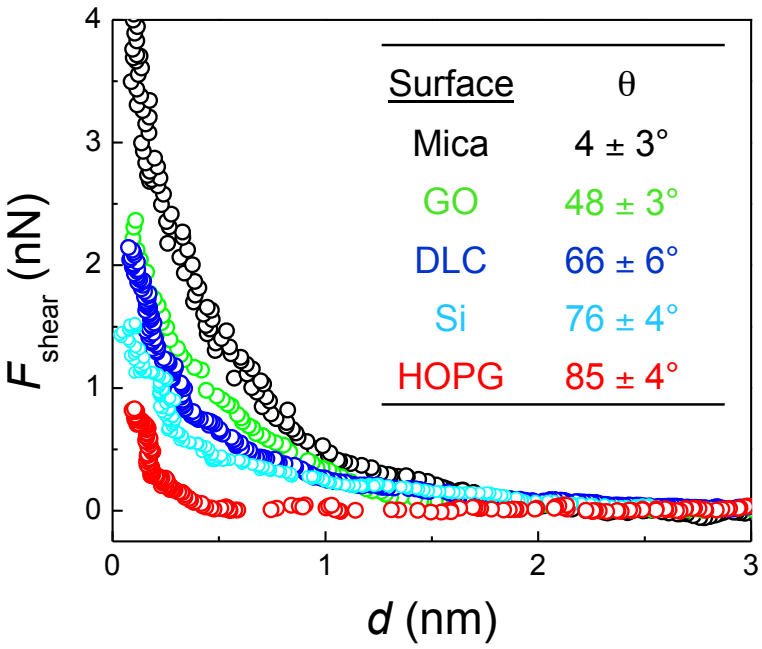

Figure 2. Lateral viscous force curves. The averaged lateral viscous force curves encountered by shearing (ν_{shear} = 900 nm/s) a nanosize AFM tip in water when approaching solid surfaces with different wettabilities. Namely, Mica (black), Graphene Oxide (green), DLC (blue), Si (cyan), and HOPG (red). The data are averaged from multiple lateral viscous force curves from d = 0.1 to 3 nm. See Supplementary Table S2. The inset shows the measured contact angles on the respective surfaces. See Supplementary Information for more details.

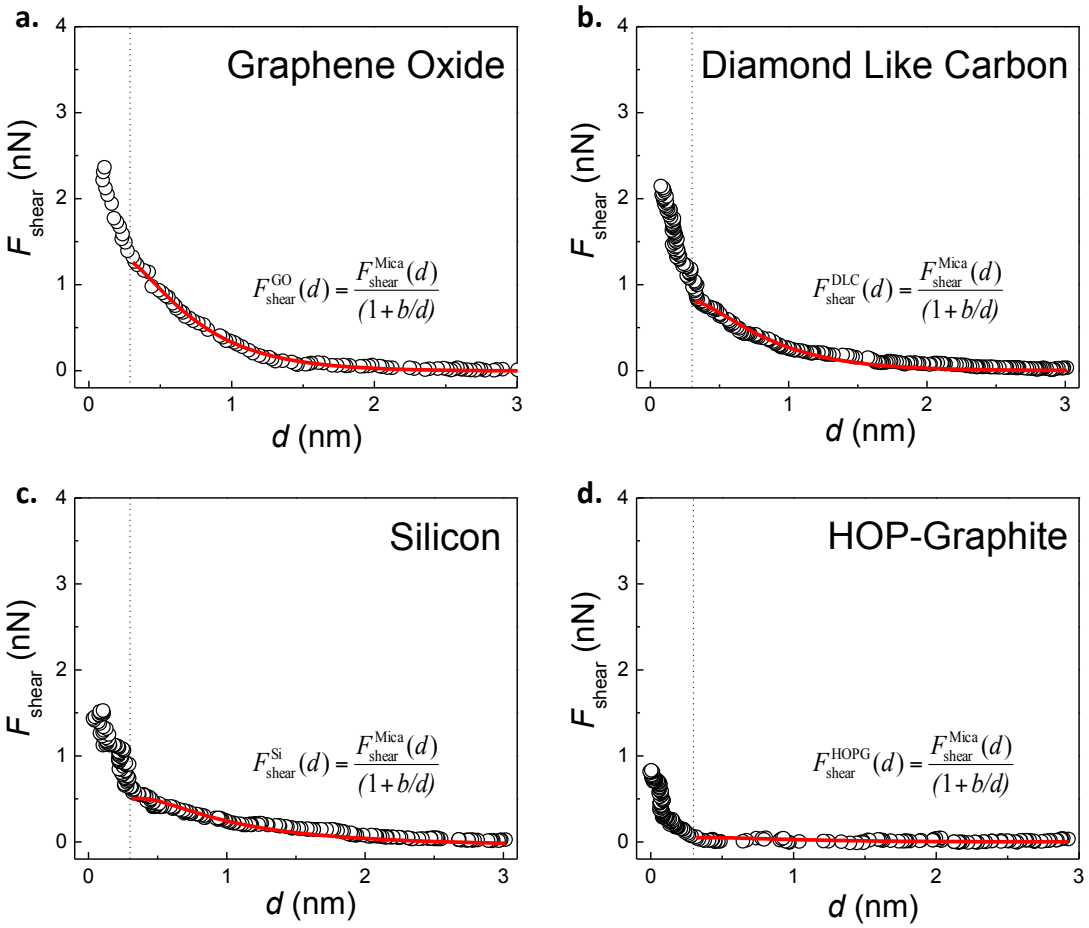

Figure 3. How slip can explain the measured effective viscosity. The lateral forces experienced by a tip approaching **a,** GO. **b,** DLC. **c,** Si. and **d,** HOPG. in water. The solid red lines in **a-d** are the fitted curves obtained by equation (4), where the only free fitting parameter is the slip length. The coefficient of determination, R, and the reduced χ^2 are determined using the Levanburg-Marquette algorithm. The obtained R is found to be 1.0 for GO, 0.99 for DLC, 0.96 for Silicon, and 0.4 for HOPG, while the reduced χ^2, which represents the deviations of the fitted curve from the experimental data, is always $< 10^{-3}$. The error bars of b shown in Figure 4 are determined from the error of averaging the lateral force curves for GO, DLC and Si. For HOPG, the error is determined from fitting using different ranges from $d \approx 0.3$ nm to $d = 3$ nm.

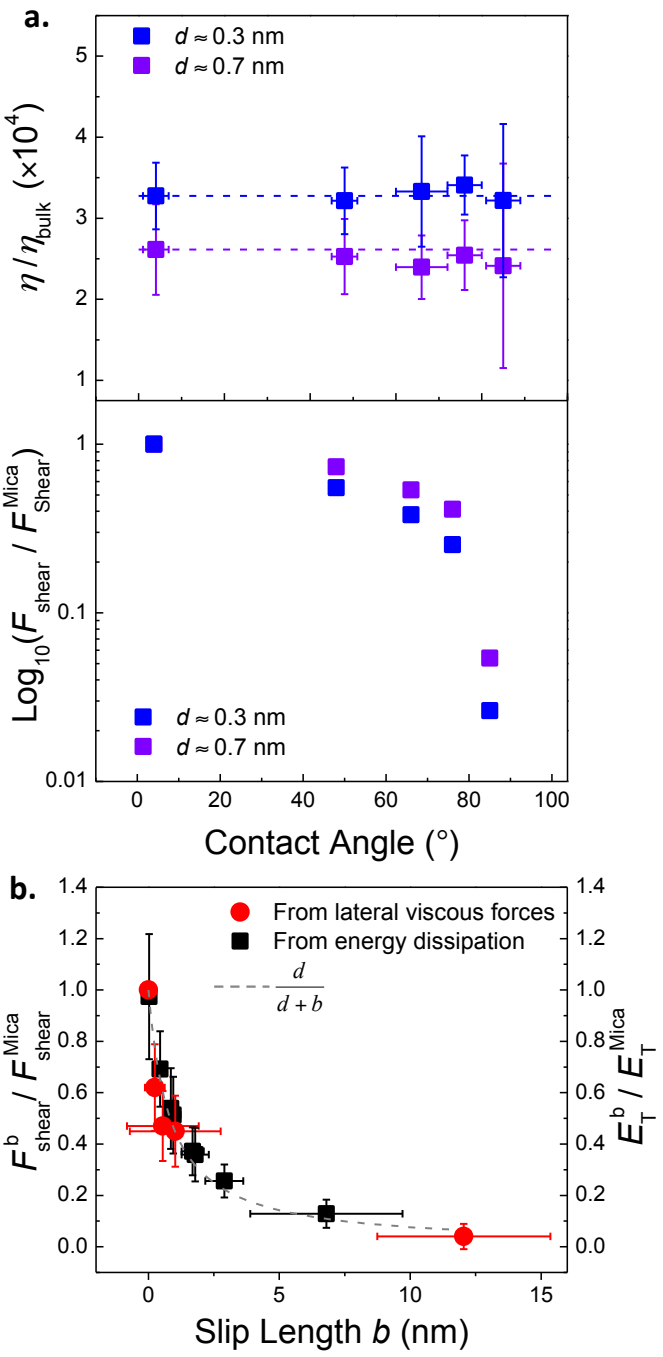

Figure 4. a, η/η_{bulk} ratio (top) and $F_{shear}/F_{shear}^{Mica}$ ratio (bottom) as a function of the water contact angle of the investigated surfaces at $d \approx 0.3$ nm and 0.7 nm. **b,** Water interfacial viscous forces ratios (circles), and energy dissipation (square) ratios as a function of the slip length for $d = 1$ nm, where b is extracted from the fitting curves illustrated in Fig. 3 using equation (4) (filled circles), and from the tip energy dissipation (filled squares) measured during dynamic mode AFM imaging in water by using equation (5). These ratios fall on a single master curve equal to $d/(b + d)$.